PHYSICAL REVIEW B **89**, 081404(R) (2014)

Bulk and surface electron dynamics in a *p*-type topological insulator $SnSb_2Te_4$

D. Niesner,[1] S. Otto,[1] V. Hermann,[1] Th. Fauster,[1] T. V. Menshchikova,[2] S. V. Eremeev,[2,3] Z. S. Aliev,[4] I. R. Amiraslanov,[4,5] M. B. Babanly,[4] P. M. Echenique,[6] and E. V. Chulkov[6,2]

[1]*Lehrstuhl für Festkörperphysik, Universität Erlangen-Nürnberg, D-91058 Erlangen, Germany*

[2]*Tomsk State University, pr. Lenina 36, 634050 Tomsk, Russia*

[3]*Institute of Strength Physics and Materials Science SB RAS, pr. Academicheskiy 2/4, 634021 Tomsk, Russia*

[4]*Baku State University, General and Inorganic Chemistry Department, Baku, Azerbaijan*

[5]*Institute of Physics, Azerbaijan National Academy of Science, Baku, Azerbaijan*

[6]*Donostia International Physics Center (DIPC), Departamento de Física de Materiales and CFM-MPC UPV/EHU, 20080 San Sebastián, Spain*

(Received 11 September 2013; revised manuscript received 16 January 2014; published 14 February 2014)

Time-resolved two-photon photoemission was used to study the electronic structure and dynamics at the surface of $SnSb_2Te_4$, a *p*-type topological insulator. The Dirac point is found 0.32 ± 0.03 eV above the Fermi level. Electrons from the conduction band minimum are scattered on a time scale of 43 ± 4 fs to the Dirac cone. From there they decay to the partly depleted valence band with a time constant of 78 ± 5 fs. The significant interaction of the Dirac states with bulk bands is attributed to their bulk penetration depth of ~3 nm as found from density functional theory calculations.

DOI: 10.1103/PhysRevB.89.081404 PACS number(s): 73.22.Pr, 73.20.−r, 79.20.Ws, 79.60.Dp

While topological insulators (TIs) are bulk insulators, they exhibit a spin-polarized metallic topological surface state (TSS) with linear dispersion (Dirac cone) [1,2]. The helical spin structure of the Dirac cone was predicted to constrain intraband scattering in the absence of spin-flipping events, resulting in long carrier lifetimes [3]. Evidence for the suppression of elastic spin-flipping scattering events was given by Fourier-transformed scanning tunneling spectroscopy [4]. Time-resolved photoemission measures the transient population of initially empty electronic states following an optical pump pulse, and therefore allows us to access electron dynamics directly in the time domain. Previous studies have focused on carrier cooling in bismuth chalcogenides which are intrinsically *n* type [5–7] and can be *p* doped by Mg [8]. These studies showed that the electron dynamics of TSSs is dominated by the bulk conduction band, but did not provide scattering rates between TSS and the conduction or valence band. Such information could be related to results obtained from transport measurements and would be important for device applications.

Complex ternary Sb_2Te_3-based alloys possess a layer structure with a van der Waals gap between Te layers and were recently proposed to exhibit a topological surface state [9–11]. However, intrinsic *p* doping of antimony-containing materials does not permit to access the Dirac point by conventional angle-resolved photoelectron spectroscopy [12] even after doping by alkali-metal atoms [13]. Angle-resolved two-photon photoemission (2PPE) uses a pump-probe process to access the unoccupied electronic states as indicated by the arrows in Fig. 1(a). Here, we show that $SnSb_2Te_4$ is a *p*-doped TI and obtain energy and dispersion of the TSS as well as bulk conduction and valence bands by 2PPE. The results agree very well with results from density functional theory (DFT) calculations. Time-resolved 2PPE is used to measure the transient population dynamics. It is dominated by refilling from the conduction band and scattering to the valence band, which is partly depleted at the present doping level. The strong interaction between bulk and surface is attributed to the large penetration depth of the TSS.

Two-photon photoemission experiments used the fundamental (1.63 eV, IR pump) and the third harmonic (4.89 eV, UV probe) of a Ti:sapphire oscillator with a repetition rate of 90 MHz. The width of the cross-correlation trace of the two pulses is 69 fs. The laser beams are *p* polarized and incident onto the sample under an angle of 45°. Spectra were recorded using a hemispherical analyzer (Omicron EA300HR with seven channeltrons) with an angular resolution of 1.6° and its energy resolution set to 34 meV (17 meV for high-resolution measurements). The sample azimuth was orientated monitoring the angular photoelectron distribution, ensuring that the plane of measurements matched the Dirac point within less than 1° corresponding to $\leqslant 0.005$ Å^{-1} at a kinetic energy of 0.35 eV. The base pressure during measurements was below 2×10^{-8} Pa. For details of the setup, see Ref. [14].

Single-crystalline $SnSb_2Te_4$ was grown from melt by the vertical Bridgman-Stockbarger method. The polycrystalline $SnSb_2Te_4$ was placed in a conical-bottom quartz ampoule, which was sealed under a vacuum better than 10^{-5} Pa. Before the growth process, the ampoule was held in the "hot" zone (~950 K) of a two-zone tube furnace for 12 h for a complete melting of the compound. Then, the charged ampoule was moved to the "cold" zone (780 K) with 1.0 mm/h. In this way, an easy-to-cleave layered single crystal with average dimensions of 2 cm in length and 0.8 cm in diameter was obtained. The grown crystal was checked by x-ray diffraction [15] and the unit-cell parameters are in good agreement with the values given in Ref. [16]. Samples were cleaved at room temperature at a base pressure below 5×10^{-7} Pa and transferred to ultrahigh vacuum within a few minutes, where they were cooled within ≈20 min to 90 K for measurements. Low-energy electron diffraction showed sharp spots with threefold symmetry.

For electronic band calculations, we use the Vienna *ab initio* simulation package [17,18] with generalized gradient

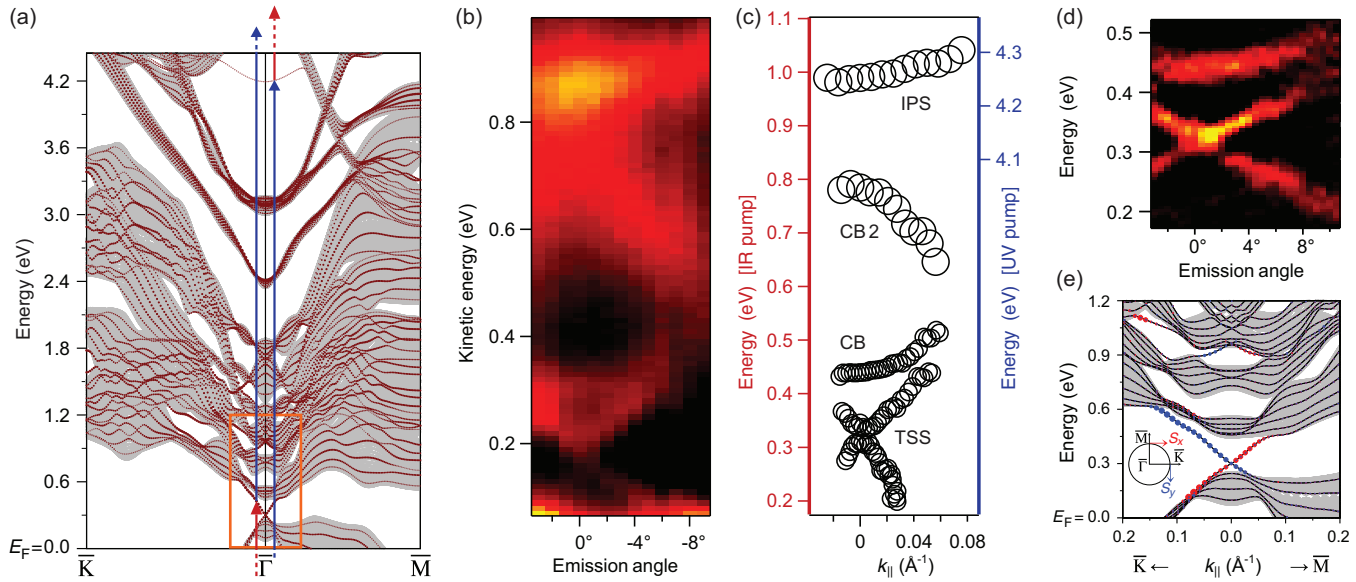

FIG. 1. (Color online) (a) Calculated band structure of $SnSb_2Te_4$. Shaded regions indicate projected bulk bands, whereas the size of the dots denotes weights of the states localized in the outermost septuple layer. The arrows indicate 2PPE processes (not to scale). (b) Angle-resolved 2PPE data of $SnSb_2Te_4$. (c) Extracted dispersion of the empty electronic states. The energy scale to the left-hand (right-hand) side corresponds to IR-pumped (UV-pumped) processes. The low-energy part of the spectrum is dominated by the UV-probed processes, and the image-potential state in the high-energy part is IR probed. (d) Second derivative of high-resolution 2PPE data in the proximity of the Dirac point. (e) Magnified view of the electronic spectrum pointed out by orange rectangle in panel (a). Dots represent weights of the states multiplied by value of in-plane spin components (red and blue colors denote opposite values of spin). The spin is oriented perpendicular to the $k_{\|}$ direction as schematically shown in inset.

approximation [19] to the exchange-correlation potential and the projector augmented wave [20,21] basis sets to solve the resulting Kohn-Sham system. The Hamiltonian contains scalar relativistic corrections, and the spin-orbit interaction is taken into account by the second variation method [22]. To simulate the semi-infinite $SnSb_2Te_4$(111), we use a slab composed of six septuple layers (SLs) separated by 30-Å vacuum space. The calculated band structure is given in Fig. 1(a). For convenience, the Dirac point has been set to 0.30 eV to match the experimental results of the *p*-doped samples.

Figure 1(b) shows 2PPE results for $SnSb_2Te_4$ as a function of kinetic energy relative to the vacuum level of the sample [23]. From the kinetic energy, the energy of the intermediate states relative to the Fermi level is obtained by adding the measured work function (4.95–5.03 eV varying slightly from cleave to cleave) and subtracting the energy of the probe photon [see arrows in Fig. 1(a)]. The feature at $E_{\mathrm{kin}} = 0.85$ eV stems from an image-potential state (IPS) 0.78 ± 0.03 eV below the vacuum level and is IR probed as will be shown by the time-resolved measurements. All other states are IR pumped (UV probed). The emission seen at the bottom of Fig. 1(b) is attributed to the valence band (VB) which is partially unoccupied. The dispersion of the IPS, the first (CB) and second conduction band (CB2), and the linearly dispersing features bridging the bulk band gap extracted from the data are presented in Fig. 1(c) on an energy scale relative to the Fermi energy E_F. The overall doping level of the surface varies from cleave to cleave with the conduction band minimum (CBM) located 0.37–0.44 eV above E_F. The upward- (downward-) dispersing first (second) conduction band as well as the linearly dispersing surface feature bridging the band gap between valence and conduction bands agree well with the calculation [Fig. 1(a)]. This shows that 2PPE on $SnSb_2Te_4$ and on other layered compounds [24] is dominated by intermediate states, and occupied initial states do not contribute. The IPS is found in the DFT calculation even though the asymptotic Coulomb potential has not been included in the computation [25]. The state has a parabolic free-electron-like dispersion and is mostly localized in the vacuum region. These findings agree with the observations for bismuth chalcogenides [8,24]. The calculations show at $\overline{\Gamma}$ two narrow bands at 2.4 and 3.1 eV [Fig. 1(a)]. Such features are absent in the spectrum of quintuple-layer-structured topological insulators of Bi_2Se_3 type and arise in the SL-structured $SnSb_2Te_4$ owing to the third element (Sn) in the central layer: The lower band at ≈2.4 eV is composed of Sn p_{xy} states, and the higher one at ≈3.1 eV is mainly determined by the Sn and inner Te atom states of p_z symmetry. Attempts to find these states by UV-UV 2PPE were not successful.

High-resolution 2PPE data around the bulk band gap are presented in Fig. 1(d) [23]. To enhance the relevant peak structures, we show the second derivative $-\frac{\partial^2}{\partial E^2} I(E,\theta)$ using a color scale suppressing negative values. The linearly dispersing features cross at 0.32 eV and have a group velocity of 3.4 ± 0.3 eV Å. They are attributed to the TSS found in the calculation of Fig. 1(e) showing a helical spin polarization. The calculations reveal the existence of another spin-polarized surface state at 0.96 eV. Such states have recently been found in other topological insulators [24,26,27]. The second spin-polarized surface state could not be confirmed by the present experiments on $SnSb_2Te_4$ due to overlap with the IPS emission.

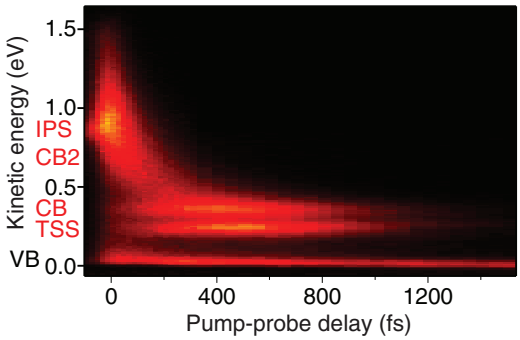

FIG. 2. (Color online) Transient population of the conduction band (CB), valence band (VB), and the topological surface state (TSS) of $SnSb_2Te_4$. The feature at $E_{kin} = 0.85$ eV is UV pumped and attributed to the image-potential state (IPS).

The temporal evolution of the transient population of the states at $\overline{\Gamma}$ excited by the IR pulse is illustrated in Fig. 2. The feature at $E_{kin} = 0.85$ eV [see also Fig. 1(b)] is attributed to the IPS. It shows a decay towards negative delay time indicating a UV-pump process with a lifetime of 17 ± 4 fs. In the following, the discussion will focus on the IR-pumped states at $E_{kin} \leqslant 0.85$ eV, i. e., $E - E_F \leqslant 0.9$ eV. The topological surface state, the first two conduction bands, and the valence band are observed within this energy window. Initially, an energetically broad electron distribution is excited in the conduction bands, which relaxes towards the conduction band minimum (CBM) with a time constant of ~240 fs. The time evolution of the TSS trails the one of the CBM, indicating that it is significantly populated by refilling from the CBM.

At fixed energy, the population decay directly reflects the lifetimes and decay rates. As a result, we observe single scattering events at these delays rather than the dynamics of a hot electron gas, which most previous studies on electron dynamics in TIs have focused on [5–7]. The dynamics can be described by a rate-equation model. The occupation n_i of state i is pumped with amplitude A_i by the Gaussian laser pulse $S(t)$. It decreases by decay with a transition rate Γ_i and increases by filling from higher-lying states with rate Γ_i^*:

$$\frac{dn_i}{dt} = A_i S(t) + \Gamma_{i+1}^* n_{i+1}(t) - \Gamma_i n_i(t). \qquad (1)$$

The total decay rate Γ_i must be larger than the rate Γ_i^* for filling the next lower-lying state unless other sources contribute. We discretize the CB into states 50 meV apart, so the ith state is located at an energy $i \times 50$ meV above the CBM. The index i runs from 0 (=CBM) to 9 ($n_{10} = 0$). Index $i = -1$ is used for the TSS below the CBM. Note that Γ^* and Γ are effective rates including scattering from and to states in the whole Brillouin zone. Figure 3(b) illustrates the model. The data (horizontal cuts of Fig. 2 summed over 50-meV energy range) are shown in Fig. 3(a) together with fits using Eq. (1). Additional measurements using smaller delay steps are given for CBM and TSS [lower panel of Fig. 3(a)]. A fit of Eq. (1) to the time-resolved spectrum of the TSS using the experimental CBM occupation n_0 as a source term yields lifetimes of 43 ± 4 fs for the CBM and 78 ± 5 fs for the TSS [squares in Fig. 3(c)].

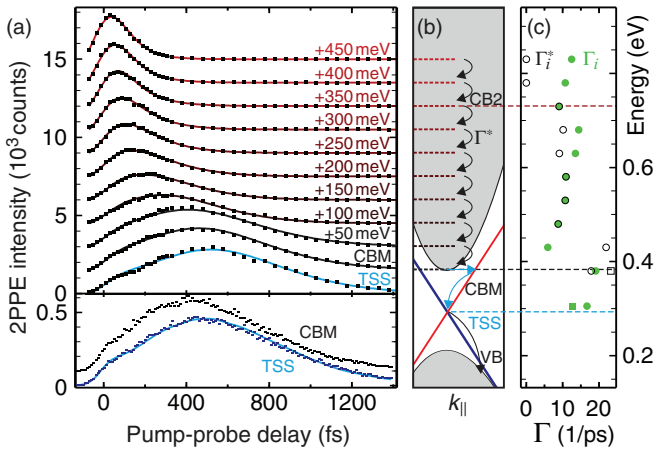

FIG. 3. (Color online) (a) Time-resolved spectra of the TSS and the CB of $SnSb_2Te_4$. The bottom panel shows data at finer time steps. Solid lines indicate fits to the data by the rate-equation model (1) illustrated in (b). (c) Extracted filling (Γ^*, open black symbols) and total decay (Γ, filled green symbols) rates. Circles and squares from data in the upper and lower panels of (a), respectively.

The scattering rates resulting from the fits using Eq. (1) to the complete data set of Fig. 3(a) are shown in Fig. 3(c). The different values obtained for the CBM and TSS from the time-resolved data in the bottom panel are due to sample degradation during the time to collect the series of energy spectra in the top panel subsequently. For most energies, the rates Γ_i and Γ_i^* agree, indicating a decay within the conduction band. An exception occurs for $\Gamma_1^* > \Gamma_1$, which can be explained by filling of the CBM by electrons from $k_{||} \neq 0$ or from the subsurface region. Within the second conduction band CB2, Γ_i^* is quite small, indicating scattering to other bands or states with $k_{||} \neq 0$. This might be related to the negative dispersion of CB2. In general, the decay rates decrease with decreasing energy in the CBs. At the CBM, the decay rate is a factor 3 larger than at 50-meV higher energy. We attribute this to quasielastic scattering (by phonons or defects) from the CBM to the TSS which is supported by the close similarity between the time-resolved spectra of the CBM and the TSS. Note that the TSS is split off from the band edges and has a wave function derived from VBM and CBM states. The occupation of the TSS decays with a time constant of 78 fs into VB states. For a higher-doped surface ($E_{CBM} - E_F = 0.42$ eV) we find a lifetime of 45 ± 4 fs due to the additional VB states available for decay at higher-doped p-type surfaces [28]. Within the experimental error of ± 4 fs, the lifetime along the TSS band is constant for $|k_{||}| \leqslant 0.025$ Å^{-1} [28]. The lifetimes τ scale within the experimental uncertainties as $\tau \propto E_{VBM}^{-2}$. The energy E_{VBM} of the VBM above E_F determines the phase space for inelastic decay of the TSS and is taken as 0.18 eV [from calculations in Fig. 1(e)] below the experimental CBM.

As a result of the helical spin structure of the TSS, long lifetimes of carriers excited into this state may be expected. The GW approximation calculations of intraband decay in the Dirac state of Bi_2Se_3 predict a lifetime of ~1 ps [3]. In contrast, for $SnSb_2Te_4$, where the Fermi level is located 0.3 eV below the Dirac point, we find a relatively short lifetime of only 78 fs. This can be attributed to scattering from the TSS

to the bulk VB. A lifetime of 6 ps has been reported for p-type-doped Bi_2Se_3 with a Fermi level position ≈ 70 meV below the Dirac point [8] and attributed to filling from the CB. In Bi_2Se_3, the top of the VB is located at 50 meV below the Dirac point [29], i.e., $E_{\mathrm{VBM}} \approx 20$ meV. The $\tau \propto E_{\mathrm{VBM}}^{-2}$ scaling used for $SnSb_2Te_4$ would yield a lifetime for Bi_2Se_3 of 3 ps similar to the theoretically predicted intraband decay rate [3] but significantly shorter than the dominating lifetime of the CB.

The scattering time from the CBM to the TSS is also quite short (43 fs). This scattering proceeds quasielastically and is followed by downward relaxation along the TSS [Fig. 3(b)]. The strong coupling between bulk CB and VB to the TSS can be explained by the sizable penetration depth of the Dirac state of two structural units [25] similar to quintuple-layered materials such as Bi_2Se_3 [30]. For $SnSb_2Te_4$, the penetration is $\sim$30 Å and leads to an enhanced scattering from or to bulk states.

The valence band is included in rate-equation model (1) only indirectly as a channel at lower energy into which the TSS electrons decay. The immediate increase of the VB intensity shown in Fig. 2 indicates that the VB is populated mainly by the pump pulse, and electrons from the CB and TSS do not increase the VB population noticeably at later times. The strong direct excitation of the VB compared to the delayed population of the CB may be explained by differences in the corresponding optical matrix elements for excitation from lower-lying valence bands. The intensity distribution of the VB intensity can be fitted well using the Boltzmann approximation of the Fermi function [31]. The temperature of VB electrons is obtained as a function of delay time and decreases linearly for delay times >100 fs [31]. The valence electrons ($\sim$0.1 eV above E_{F}) exchange energy predominantly among themselves or with lattice vibrations. The situation can be treated in a two-temperature model [32] and yields an electron-phonon coupling parameter $6.2 \pm 0.7 \times 10^{-5}\, k/\mathrm{fs}$ [31]. This value translates [31,33] to an electron-phonon mass enhancement parameter $\lambda = 0.15$ which compares well to $\lambda = 0.1$ derived from transport measurements in the related compound $GeSb_2Te_4$ [34].

In summary, we examined by two-photon photoelectron spectroscopy the unoccupied states of p-type topological insulator $SnSb_2Te_4$. The Dirac cone is found 0.32 eV above the Fermi level with a group velocity of 3.4 eV Å. At 4.2 eV, an image-potential state with a lifetime of 17 fs was identified. The DFT calculations support these experimental findings. The time scales for scattering in and out of the topological surface state are below 100 fs. We attribute the domination of the bulk scattering channels for the decay to the depopulated bulk valence states for the strongly p-doped sample and the deep bulk penetration of the topological state. The scattering rate from the topological surface state to the valence band scales approximately with the square of the energy of the VBM above E_{F}. For applications of TIs based on transport, the Fermi level should be in the band gap to minimize carrier scattering.

The authors thank I. A. Nechaev for helpful discussions. We acknowledge partial support from the Basque Country Government, Departamento de Educación, Universidades e Investigación (Grant No. IT-366-07), the Spanish Ministerio de Ciencia e Innovación (Grant No. FIS2010-19609-C02-00), the Ministry of Education and Science of Russian Federation (Grant No. 2.8575.2013), the Russian Foundation for Basic Research (Grant No. 13-02-12110_ofi_m), and Science Development Foundation under the President of the Republic of Azerbaijan [Grant No. EIF-2011-1(3)-82/69/4-M-50].

[1] L. Fu, C. L. Kane, and E. J. Mele, Phys. Rev. Lett. **98**, 106803 (2007).
[2] L. Fu and C. L. Kane, Phys. Rev. B **76**, 045302 (2007).
[3] I. A. Nechaev and E. V. Chulkov, JETP Lett. **96**, 480 (2012).
[4] P. Roushan, J. Seo, C. V. Parker, Y. S. Hor, D. Hsieh, D. Qian, A. Richardella, M. Z. Hasan, R. J. Cava, and A. Yazdani, Nature (London) **460**, 1106 (2009).
[5] M. Hajlaoui, E. Papalazarou, J. Mauchain, G. Lantz, N. Moisan, D. Boschetto, Z. Jiang, I. Miotkowski, Y. P. Chen, A. Taleb-Ibrahimi, L. Perfetti, and M. Marsi, Nano Lett. **12**, 3532 (2012).
[6] Y. H. Wang, D. Hsieh, E. J. Sie, H. Steinberg, D. R. Gardner, Y. S. Lee, P. Jarillo-Herrero, and N. Gedik, Phys. Rev. Lett. **109**, 127401 (2012).
[7] A. Crepaldi, B. Ressel, F. Cilento, M. Zacchigna, C. Grazioli, H. Berger, P. Bugnon, K. Kern, M. Grioni, and F. Parmigiani, Phys. Rev. B **86**, 205133 (2012).
[8] J. A. Sobota, S. Yang, J. G. Analytis, Y. L. Chen, I. R. Fisher, P. S. Kirchmann, and Z.-X. Shen, Phys. Rev. Lett. **108**, 117403 (2012).
[9] S. V. Eremeev, G. Landolt, T. V. Menshchikova, B. Slomski, Y. M. Koroteev, Z. S. Aliev, M. B. Babanly, J. Henk, A. Ernst, L. Patthey, A. Eich, A. A. Khajetoorians, J. Hagemeister, O. Pietzsch, J. Wiebe, R. Wiesendanger, P. M. Echenique, S. S. Tsirkin, I. R. Amiraslanov, J. H. Dil, and E. V. Chulkov, Nat. Commun. **3**, 635 (2012).
[10] T. V. Menshchikova, S. V. Eremeev, and E. V. Chulkov, Appl. Surf. Sci. **267**, 1 (2013).
[11] M. G. Vergniory, T. V. Menshchikova, S. V. Eremeev, and E. V. Chulkov, Appl. Surf. Sci. **267**, 146 (2013).
[12] D. Hsieh, Y. Xia, D. Qian, L. Wray, F. Meier, J. H. Dil, J. Osterwalder, L. Patthey, A. V. Fedorov, H. Lin, A. Bansil, D. Grauer, Y. S. Hor, R. J. Cava, and M. Z. Hasan, Phys. Rev. Lett. **103**, 146401 (2009).
[13] C. Seibel, H. Maaß, M. Ohtaka, S. Fiedler, C. Jünger, C.-H. Min, H. Bentmann, K. Sakamoto, and F. Reinert, Phys. Rev. B **86**, 161105 (2012).
[14] K. Boger, T. Fauster, and M. Weinelt, New J. Phys. **7**, 110 (2005).
[15] A Bruker D8 ADVANCE diffractometer with Cu–Kα radiation was used. The unit-cell parameters were calculated with EVA and TOPAS V3.0 software.
[16] O. Oeckler, M. N. Schneider, F. Fahrnbauer, and G. Vaughan, Solid State Sci. **13**, 1157 (2011).
[17] G. Kresse and J. Hafner, Phys. Rev. B **48**, 13115 (1993).
[18] G. Kresse and J. Furthmüller, Comput. Mater. Sci. **6**, 15 (1996).
[19] J. P. Perdew, K. Burke, and M. Ernzerhof, Phys. Rev. Lett. **77**, 3865 (1996).

[20] P. E. Blöchl, Phys. Rev. B **50**, 17953 (1994).
[21] G. Kresse and D. Joubert, Phys. Rev. B **59**, 1758 (1999).
[22] D. D. Koelling and B. N. Harmon, J. Phys. C: Solid State Phys. **10**, 3107 (1977).
[23] See Supplemental Material at http://link.aps.org/supplemental/10.1103/PhysRevB.89.081404 for original spectra of Figs. 1(a) and 1(d). All data were recorded after reaching a stable level of the work function. The value after cleaving and transferring the sample to the spectrometer is above 5.5 eV and decreases within a hour to a stationary level around 5.0 eV. Likewise, the energy of the Dirac point varies slightly. A similar behavior is found for bismuth chalcogenides [24].
[24] D. Niesner, T. Fauster, S. V. Eremeev, T. V. Menshchikova, Y. M. Koroteev, A. P. Protogenov, E. V. Chulkov, O. E. Tereshchenko, K. A. Kokh, O. Alekperov, A. Nadjafov, and N. Mamedov, Phys. Rev. B **86**, 205403 (2012).
[25] See Ref. [23] for probability densities of IPS and TSS.
[26] S. V. Eremeev, I. V. Silkin, T. V. Menshchikova, A. P. Protogenov, and E. V. Chulkov, JETP Lett. **96**, 780 (2013).
[27] J. A. Sobota, S.-L. Yang, A. F. Kemper, J. J. Lee, F. T. Schmitt, W. Li, R. G. Moore, J. G. Analytis, I. R. Fisher, P. S. Kirchmann, T. P. Devereaux, and Z.-X. Shen, Phys. Rev. Lett. **111**, 136802 (2013).
[28] See Ref. [23] for time-resolved data from a higher-doped surface.
[29] I. A. Nechaev, R. C. Hatch, M. Bianchi, D. Guan, C. Friedrich, I. Aguilera, J. L. Mi, B. B. Iversen, S. Blügel, P. Hofmann, and E. V. Chulkov, Phys. Rev. B **87**, 121111 (2013).
[30] S. V. Eremeev, M. G. Vergniory, T. V. Menshchikova, A. A. Shaposhnikov, and E. V. Chulkov, New J. Phys. **14**, 113030 (2012).
[31] See Ref. [23] for details of the fitting procedure.
[32] S. I. Anisimov, B. L. Kapeliovich, and T. L. Perel'man, Zh. Eksp. Teor. Fiz **66**, 776 (1974) [Sov. Phys.–JETP **39**, 375 (1974)].
[33] P. B. Allen, Phys. Rev. Lett. **59**, 1460 (1987).
[34] N. P. Breznay, H. Volker, A. Palevski, R. Mazzarello, A. Kapitulnik, and M. Wuttig, Phys. Rev. B **86**, 205302 (2012).